

## SUPPORTING INFORMATION

### Computational Investigation of Microgels: Synthesis and Effect of the Microstructure on the Deswelling Behavior

Angel J. Moreno<sup>1,2,\*</sup> and Federica Lo Verso<sup>3,2</sup>

<sup>1</sup>*Centro de Física de Materiales (CSIC,  
UPV/EHU) and Materials Physics Center MPC,  
Paseo Manuel de Lardizabal 5, E-20018 San Sebastián, Spain.*

<sup>2</sup>*Donostia International Physics Center,  
Paseo Manuel de Lardizabal 4, 20018 San Sebastián, Spain.*

<sup>3</sup>*Department of Physics, Chemistry and Pharmacy,  
University of Southern Denmark, Campusvej 55, Odense M 5230, Denmark*

---

\*Corresponding author: [angeljose.moreno@ehu.es](mailto:angeljose.moreno@ehu.es)

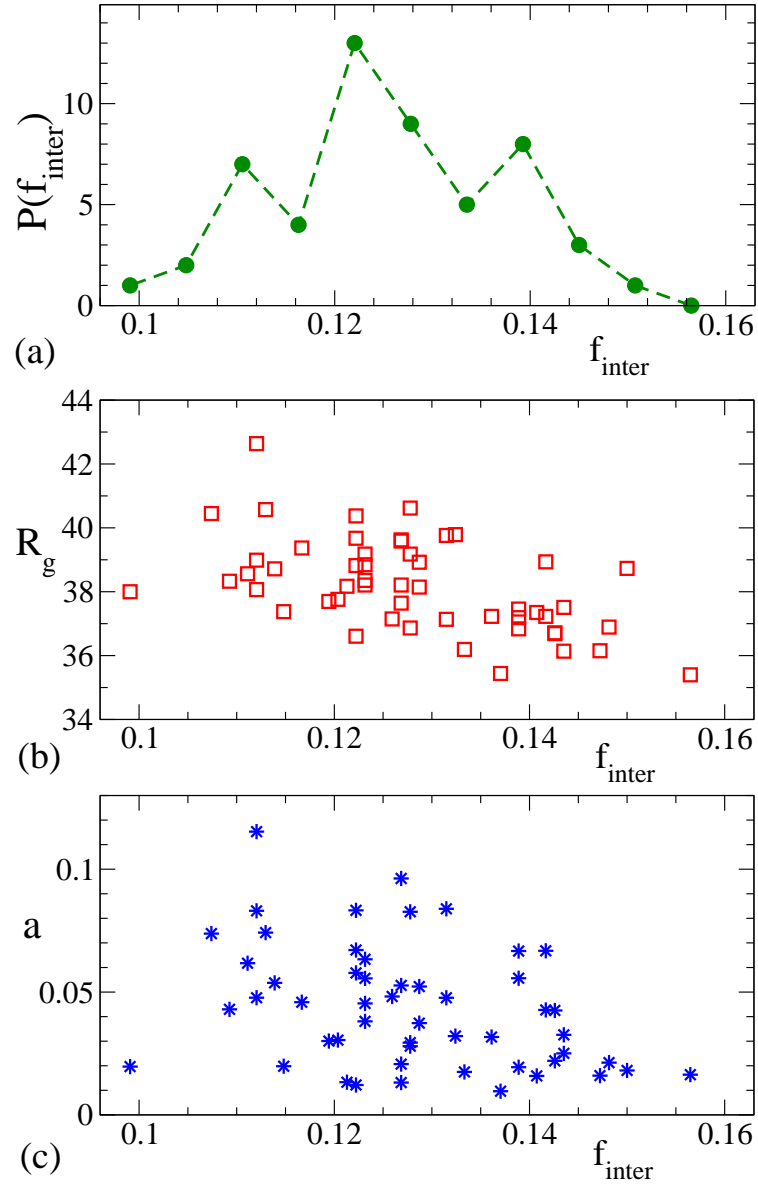


Figure S1: Panel (a): distribution of the fraction of intermolecular bonds in the disordered microgels. Panels (b) and (c): correlations of the time-averaged radii of gyration and asphericities with the fractions of intermolecular bonds.

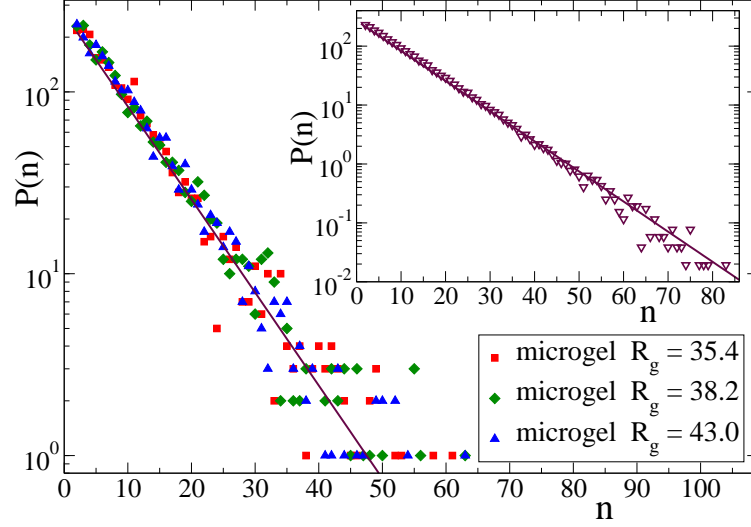


Figure S2: Distribution  $P(n)$  of strand lengths between nearest cross-links for the small, middle and large disordered microgels (main panel), and for the whole ensemble of disordered microgels (inset). Symbols are simulation data. The lines are the Flory's prediction,  $P(n) = N_t f^2 (1 - 2f)^{n-1} (1 - f)^{-n}$ .

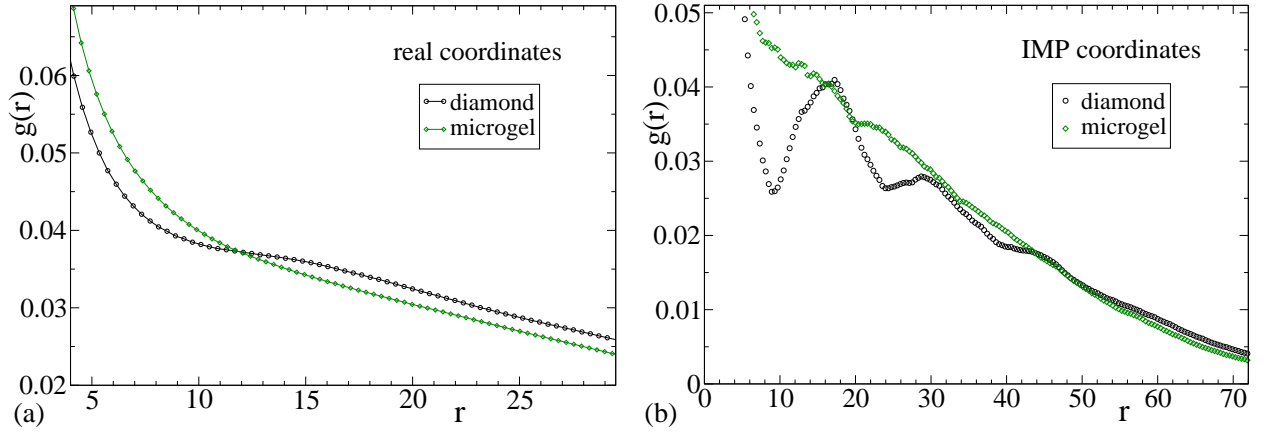


Figure S3: Radial distribution function of the diamond (circles) and the middle-size disordered microgel (diamonds). Panels (a) and (b) are results obtained by using real and IMP coordinates, respectively.

## FUZZY SPHERE MODEL

The expression of the fuzzy sphere model for the form factor is:

$$w(q) = \left[ \frac{3[\sin(qR') - qR' \cos(qR')]}{q^3 R'^3} \exp\left(-\frac{q^2 \sigma_s^2}{2}\right) \right]^2 + \frac{I(0)}{1 + q^2 \xi^2} \quad (1)$$

In this equation  $R'$  is the radius of the constant-density core and  $2\sigma_s$  (smearing parameter) represents the thickness of the outer shell. The Lorentzian term represents the scattering (with intensity  $I(0)$ ) from the network fluctuations, of correlation length  $\xi$ . The corresponding expression of the fuzzy sphere model for the monomer density profile  $\rho(r)$  (where  $r$  is the distance of the monomer to the macromolecular center-of-mass) is given by:

$$\frac{\rho(r)}{\rho(0)} = \begin{cases} 1 & r < R' - 2\sigma_s \\ 1 - \frac{(r - R' + 2\sigma_s)^2}{8\sigma_s^2} & R' - 2\sigma_s \leq r < R' \\ \frac{(R' - r + 2\sigma_s)^2}{8\sigma_s^2} & R' \leq r < R' + 2\sigma_s \\ 0 & r \geq R' + 2\sigma_s \end{cases} \quad (2)$$

The values of the fuzzy-sphere parameters  $R'$ ,  $\sigma_s$ ,  $\xi$  and  $I(0)$  for the analyzed systems are given in Table S1.

System		$R'$	$\sigma_s$	$\xi$	$I(0)$
Diamond	$R_g = 37.3$ (real coord.)	46.0	5.8	2.7	0.0015
Disordered I	$R_g = 35.4$ (real coord.)	39.3	8.8	6.1	0.0056
Disordered II	$R_g = 38.2$ (real coord.)	43.5	10.0	6.7	0.0075
Disordered III	$R_g = 43.0$ (real coord.)	40.0	16.0	16.3	0.039
Diamond	$R_g = 37.3$ (IMP)	46.0	3.7	0.57	0.00097
Disordered II	$R_g = 38.2$ (IMP)	43.2	8.5	1.7	0.0034

Table S1: Parameters of the fuzzy sphere model for the analyzed systems.

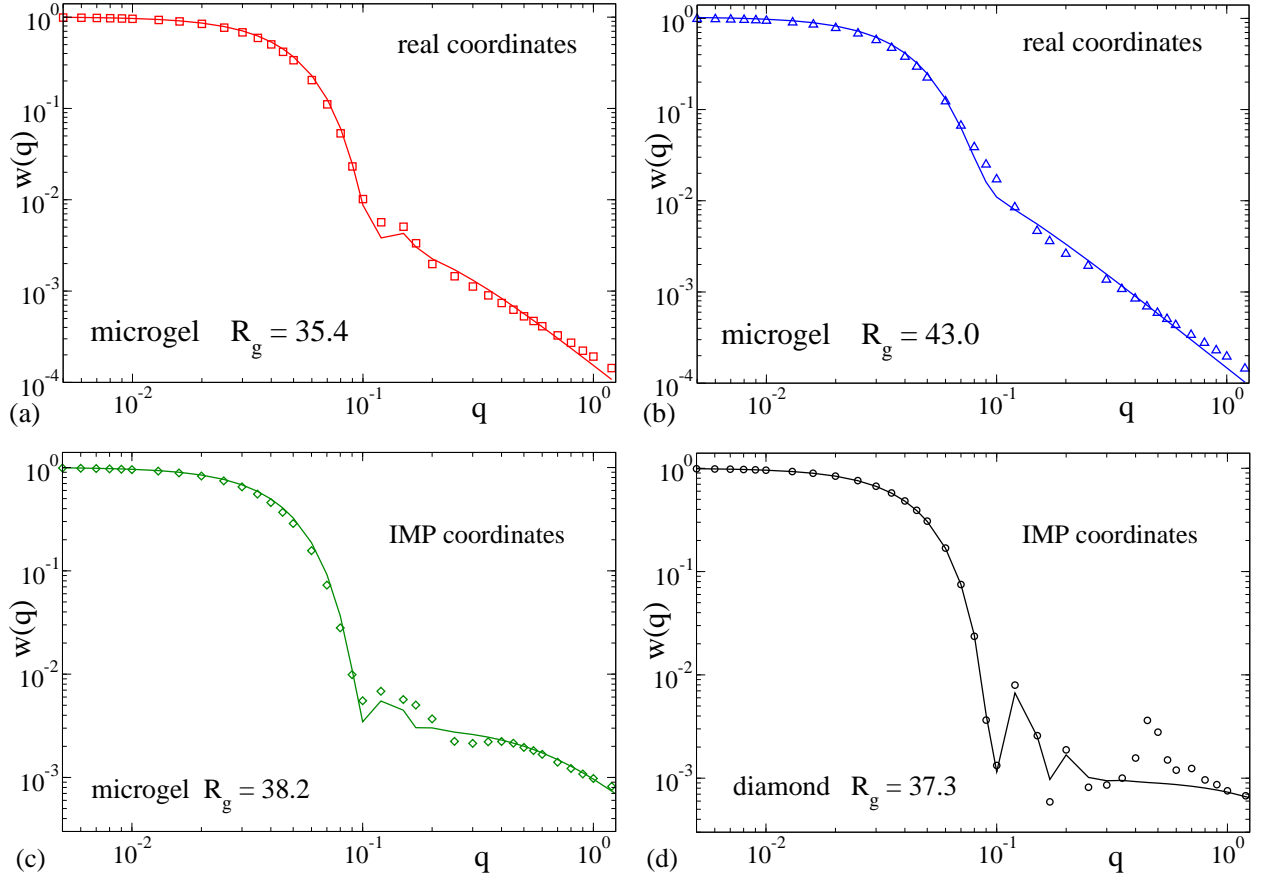


Figure S4: Symbols: Form factors of the small (a), large (b), middle (c) disordered microgels, and of the diamond microgel (d). Panels (a) and (b) are results obtained by using real coordinates. IMP coordinates are used in panels (c) and (d). Lines: Fits to the fuzzy sphere model. The numerical values of the model parameters are given in Table S1.

## EULER CHARACTERISTIC

In order to further characterize the microgel structure and highlight the differences with pre-constructed ordered networks we utilize the Euler characteristic  $\chi$ , namely one of the four scalar Minkowski functionals [1, 2] that characterize a given surface embedded in three dimensions. This morphometric approach is able to take into account multi-body correlations among the constituent monomers and give details on their spatial arrangement. The coefficient itself is proportional to the integral Gaussian curvature and its value is not subject to continuous, topology-preserving deformations of the surface. In three dimensions  $\chi = \mathcal{N}_D + \mathcal{N}_C - \mathcal{N}_T$ , where  $\mathcal{N}_D$  is the number of disconnected aggregates,  $\mathcal{N}_C$  the number of enclosed cavities and  $\mathcal{N}_T$  the number of perforations (tunnels) that percolate through the system. In order to compute  $\chi$  we follow the procedure described in Ref. [3]. The system box is discretized into a cubic lattice, of spacing  $d$ . Each lattice site is surrounded by a Wigner-Seitz cell, in this case an elementary cube having the size of the lattice constant. We then consider the surfaces  $\mathcal{S}(R)$  formed by spheres with a radius  $R$  located at the centers of every monomer. We denote each lattice site inside  $\mathcal{S}(R)$  as ‘filled’ and all others sites as ‘empty’.  $R$  denotes the relevant length scale: for small values of  $R$  we have a collection of disjoint spheres. While increasing  $R$ , some of the spheres merge, and progressively form rings and cavities. For  $R$  large enough the collection of spheres will fully occupy the space containing the molecule, and the ultimate value  $\chi = 1$  is reached. For every chosen  $\mathcal{S}(R)$  family, the Euler characteristic is computed as explained in Ref. [1]. Due to the discretized nature of the surface  $\mathcal{S}(R)$  obtained with this procedure, we choose a lattice spacing  $d$  sufficiently small to avoid artifacts arising from the discretization.

Figure S5a shows  $\chi(R)$  for the real coordinates of the diamond (averaged over several run steps) and the disordered microgel. In the case of the disordered microgel, statistics have been improved by averaging over 5 different configurations and several steps each. The data are normalized by the total number of monomers,  $N_t$ , of the respective microgel. Therefore, since in the limit  $R \rightarrow 0$  the surface  $\mathcal{S}(R)$  is constituted by  $N_t$  disconnected spheres,  $\chi(0) = 1$ . By increasing  $R$  the merging of the sphere surfaces leads to the formation of rings, which contribute negatively (as tunnels) to the Euler characteristic. This results in a minimum at a distance slightly above the monomer radius. As the sphere radius  $R$  goes on growing up, the perforations progressively shrink and vanish, or become enclosed cavities

isolated from the empty space. Thus, the positive contributions of the emerging cavities and the cancelation of the negative contributions of the tunnels lead to an increase of the Euler characteristic. For large  $R$  the whole structure merges into a single solid sphere without tunnels or cavities, reaching the final value  $\chi = 1/N_t \approx 4.6 \times 10^{-5}$ . A closer inspection at intermediate distances reveals different features in the  $\chi(R)$  of the diamond and the disordered microgel. Within statistics, a monotonous increase of  $\chi(R)$  is observed for the disordered microgel. However, the interplay of emerging cavities and vanishing perforations leads to a broad maximum at  $R \sim 5$  for the diamond microgel (see inset in Figure S5a). In a network with well-defined length scales (between nearest nodes, next-to-nearest ones, etc), the vanishment of the negative contributions from the tunnels associated to a given length scale (and the emergence of cavities originating from the enclosed tunnels) will lead to a steep increase of  $\chi$  when  $R$  probes such a length scale, and eventually a maximum in  $\chi$ . Due to the twist of the polymer chains the maximum is not pronounced, but still reflects the underlying regular diamond network. Due to the absence of such a regular structure for the disordered microgel, no characteristic length scale can be solved by  $\chi(R)$  in its real-coordinate configurations.

Figure S5b displays the Euler characteristics of the corresponding IMP coordinates of the diamond and disordered microgel. Data correspond to the average over 5 different IMP configurations. Due to the strong overlap of bonded monomers in the IMP coordinates, the merging of the fully disconnected spheres into rings (and the associated minimum in  $\chi(R)$ ) occurs at  $R \ll 1$ . The perforations associated to the small rings quickly vanish with growing  $R$ , resulting in a steep increase from the minimum. This is followed by a well-defined plateau. Because of the rod-like character of the strands in the IMP configurations, the growth of the spheres in this regime is much less sensitive to fluctuations and wiggles than in the real-coordinate configurations. Thus, no significant vanishment of perforations or emergence of cavities occurs by increasing  $R$  over a significant range, and the Euler characteristic is almost unaffected up to  $R \approx 6$  and  $R \approx 4$  for the diamond and microgel network, respectively. This feature is fully expected for a regular network, but is a remarkable one for the disordered one. Figure S5b demonstrates that the IMP construction in combination with the Euler characteristic is able to detect a certain underlying mesh size in the disordered microgel network.

As expected, vanishment of perforations and emergence of cavities start to arise at longer

$R$  and, as observed before for the real coordinates, the  $\chi(R)$  of the IMP configurations increases. In the diamond network the peak for the IMP coordinates is narrower than its counterpart for the real ones and is located at larger distances. This feature originates from the averaging out of the fluctuations and wiggles in the IMP, which shifts the closure and vanishment of perforations to larger values of  $R$ . In the disordered microgel the Euler characteristics for the real and IMP coordinates show negligible differences for  $R > 4$ . No further characteristic length scales of the disordered network are probed by increasing the sphere radius  $R$ , and  $\chi(R)$  grows smoothly until its final value  $\chi = 1/N_t$ .

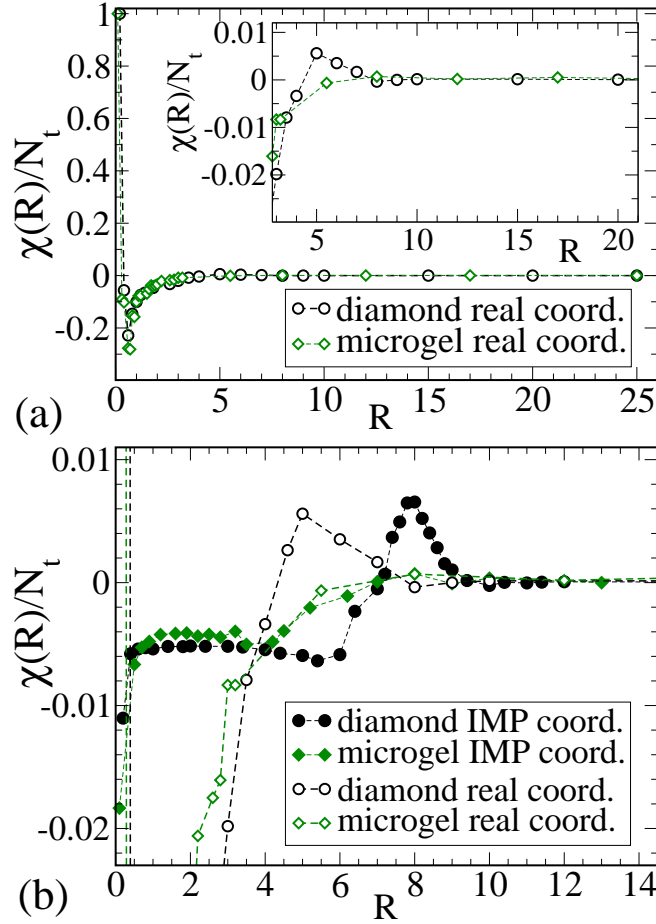


Figure S5: Euler characteristic  $\chi(R)$  for the diamond and for a middle-size disordered microgel. Panel (a) shows data for the real coordinates. The inset highlights the differences between both systems at  $R \sim 5$ . Panel (b) compares the  $\chi(R)$  of both systems, for the real and the IMP coordinates, in the relevant range of distances probing the network structure.



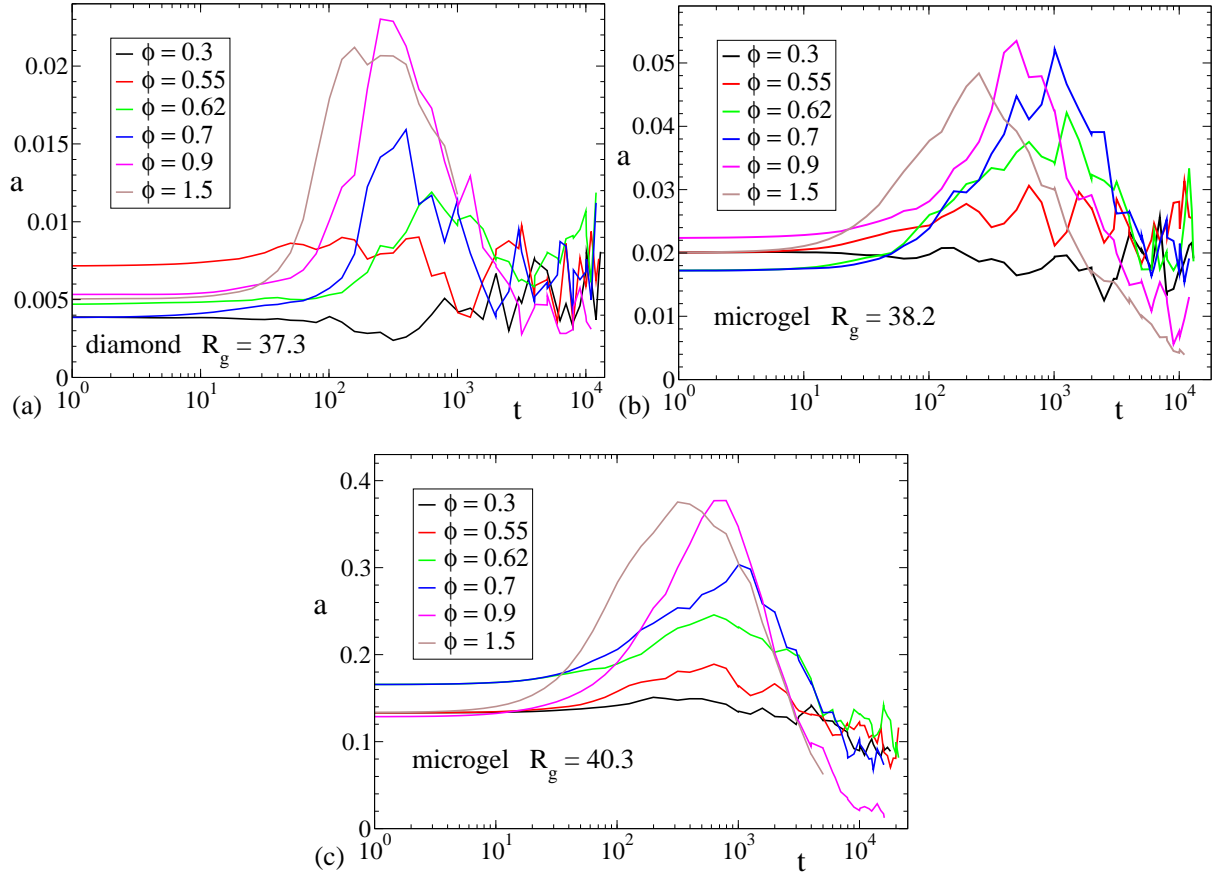


Figure S6: Time dependence of the asphericity parameter during the collapse of the diamond and two representative disordered microgels, at different  $\phi$ -values.

- 
- [1] C. N. Likos, K. R. Mecke and H. Wagner, *J. Chem. Phys.*, 1995, **102**, 9350–9361.
  - [2] N. Hoffmann, F. Ebert, C. N. Likos, H. Löwen and G. Maret, *Phys. Rev. Lett.*, 2006, **97**, 078301.
  - [3] A. Sanchez-Sanchez, S. Akbari, A. J. Moreno, F. Lo Verso, A. Arbe, J. Colmenero and J. A. Pomposo, *Macromol. Rapid Commun.*, 2013, **34**, 1681–1686